12 Jan 87 Conference Presentation

Dynamic Stall Wake Interaction With a Trailing Airfoil

TA 2307-F1-38

J. Walker

F.J. Seiler Research Laboratory
USAF Academy CO 80840-6528

FJSRL-PR-90-0005

Distribution Unlimited

Experiments were conducted with tandem NACA 0015 airfoils placed in a wind tunnel 0.5 chord lengths apart. The leading airfoil was pitched about its quarter-chord axis at high constant rates from zero to 60 degrees incidence at chord Reynolds numbers from 50,000 to 200,000. These motions produced energetic dynamic stall vortex flows which impinged on the trailing airfoil fixed at zero degrees geometric angle of attack. Smoke-wire flow visualization and dynamic surface pressure measurement experiments were performed to study the effects of the unsteady vortical wakes on the trailing airfoil. The dynamic stall vortices produced by the pitching airfoil elicited complex, time-dependent secondary flow structures around the trailing airfoil which in turn produced large dynamic loads. These large transient loads may pose significant problems to the designers of control systems of aircraft generating or encountering such unsteady vortical flow structures.

flow visualization
dynamic loads
vortices

11

UNCLASSIFIED UNCLASSIFIED UNCLASSIFIED NONE

AIAA'87

AIAA-87-0239

Dynamic Stall Wake Interaction With a Trailing Airfoil

J. Walker, Frank J. Seiler Research Laboratory, USAF Academy, Co.

AIAA 25th Aerospace Sciences Meeting

January 12-15, 1987/Reno, Nevada

DYNAMIC STALL WAKE INTERACTION WITH A TRAILING AIRFOIL

John M. Walker*
Frank J. Seiler Research Laboratory
USAF Academy, Colorado Springs, Colorado 80840-6528

Abstract

Experiments were conducted with tandem NACA 0015 airfoils placed in a wind tunnel 0.5c apart. The leading airfoil was pitched about its quarter-chord axis at high constant rates from zero to sixty degrees incidence at chord Reynolds numbers from 50000 to 200000. These motions produced energetic dynamic stall vortex flows which impinged on the trailing airfoil fixed at zero degrees geometric angle of attack. Smoke-wire flow visualization and dynamic surface pressure measurement experiments were performed to study the effects of the unsteady vortical wakes on the trailing airfoil. The dynamic stall vortices produced by the pitching airfoil elicited complex, time-dependent secondary flow structures around the trailing airfoil which in turn produced large dynamic loads. These large transient loads may pose significant problems to the designers of control systems of aircraft generating or encountering such unsteady vortical flow structures.

Nomenclature

c	Airfoil chord
C_d	Airfoil pressure drag coefficient
C_l	Airfoil lift coefficient
$C_{mc/4}$	Airfoil quarter-chord moment coefficient
C_p	Airfoil pressure coefficient = $(P-P_\infty)/q_\infty$
R_e	Reynolds number = $U_\infty c/\nu$
t	Time
U_∞	Freestream velocity
$\dot{\alpha}$	Pitch rate
α^+	Non-dimensional pitch rate = $\dot{\alpha} c/U_\infty$
ν	Kinematic viscosity
τ	Non-dimensional time = $t\ U_\infty / c$

Introduction

With the advent of high speed computers the field of unsteady aerodynamics has been the subject of intense study from both a computational and an experimental standpoint over the past couple of decades.[1,2] In particular, the areas of unsteady separated and vortex flows have received special emphasis.[3] Initially, researchers[4] were concerned with mitigating the adverse effects of the associated dynamic overshoots in aerodynamic loading usually followed by catastrophic stall. More recently, however, studies[5,6,7] have been performed to gain a better understanding of forced unsteady vortex flows so that these large forces can be exploited for enhanced aircraft maneuverability.

Coupled with the production of large aerodynamic forces through the generation of energetic vortical flows is the effect of impingement of these flows on downstream aerodynamic surfaces. Recent experimental studies have included investigations of blade-vortex interactions with streamwise[8,9] and two-dimensional spanwise[10,11,12,13,14] vortices, where dynamic lift coefficients have been measured from 1.1 to 2.6 times the steady flow values. Analytic[15] and computational[11,12,16,17,18] efforts have reported similar results. The experimental two-dimensional vortex impingement studies have, however, been limited to either dynamic stall vortex generation by relatively low amplitude harmonic motions or by passing a blade through a longitudinal vortex with the span parallel to the vortex core. The advent of modern high performance aircraft such as the X-29 which has control surfaces which are capable of producing forced unsteady vortex flows, the planned development of aircraft whose high maneuvering capabilities may produce dynamic stall, and the potential development of future aircraft whose extreme maneuverability may result from designs incorporating large amplitude unsteady vortices, have provided motivation for understanding the impact of these flows on downstream surfaces.

In this paper experimental investigations were carried out to examine unsteady vortical wake interactions with a trailing airfoil resulting from dynamic stall vortex generation by large amplitude, high rate pitching motions.

Methods

These experiments were conducted in the low turbulence 2 ft x 2 ft low speed wind tunnel at the University of Colorado. The experimental arrangement consisted of two full span, 6 inch chord NACA 0015 airfoils mounted in tandem on the tunnel centerline, initially at zero degrees incidence. The trailing airfoil was mounted statically with its leading edge 0.5c aft of the initial position of the trailing edge of the leading airfoil.

The leading airfoil was pitched about its quarter chord at constant rates from angles of attack of zero to sixty degrees and held. Pitch rates were varied from 230 to 920 degrees per second at chord Reynolds numbers from 50000 to 200000 in accordance with the test matrix shown in Table 1. The numbers within the matrix indicate the associated non-dimensional pitch rate, α^+. These parameters were selected based on previous studies.[7,14,19,20]

Table 1
Test Matrix

$\dot{\alpha}$ (deg/sec)	230	460	920
U_∞ (ft/sec)			
20	0.1	0.2	0.4
40	0.05	0.1	0.2
80	0.025	0.05	0.1

*Chief, Aerospace Mechanics Division
Member, AIAA

The primary test article, the trailing airfoil, was subjected to the vortex-dominated unsteady wakes generated by the leading airfoil. Two techniques were used to examine the flow about the trailing airfoils: stroboscopic smoke-wire flow visualization for the three cases at the free stream velocity of 20 fps and surface pressure measurements for the entire test matrix. The flow visualization provided insight into the flow field dynamics while the instantaneous pressure measurements determined the airfoil loadings induced by the unsteady wake passage. The pressure airfoil was instrumented with 18 Endevco 8507-2 miniature pressure transducers close-coupled to a single surface, effectively providing 36 pressure locations on the airfoil. Each pressure port was sequentially sampled 200 times over the sample period - the period determined by the start of the leading airfoil motion and the convection time of the elicited dynamic stall vortex over the trailing airfoil. Each event was repeated 25 times and an ensemble average taken. Further information on the instrumentation and data acquisition is detailed elsewhere.[19]

Results

Previous studies[7,20] have examined the flowfields about airfoils pitching at high rates to large angles of attack. In these, the existence of energetic dynamic stall vortices elicited by the pitching airfoils were shown, and vortex dynamics were quantified as functions of the non-dimensional pitch rate. Others[6,19,20,21,22] have quantified the resulting forces on the airfoil as functions of pitch rate and Reynolds number. They have found that for relatively high Reynolds numbers (i.e., Re 10^4), these flowfields are relatively Reynolds number independent, and that the non-dimensional pitch rate, α^+, is a dynamic similarity parameter. Theoretical confirmation of this has been provided by Cook[23] who showed the relative importance of Reynolds number and the non-dimensional pitch rate which is introduced through the boundary conditions. For NACA 0015 airfoils, maximum transient lift (and pressure drag) coefficients exceeded the maximum static value by factors from two to six on a curve of decreasing slope over a range of non-dimensional pitch rates from 0.05 to 0.8.

The wake structures resulting from pitching airfoils are not, however, merely functions of the dynamic stall vortices shed downstream. As the airfoil begins to pitch up, the wake transitions from a thin layer of alternately shed vortices to a wider region of "starting vortices" continually shed from the lower (pressure) airfoil surface opposite in sense to the airfoil pitching motion. These "starting vortices" rotate in a widening separated wake region emanating from the area of the upper (suction) surface of the airfoil near the trailing edge. Coincident with the shedding of the starting vortices is the rapid accumulation of vorticity around the airfoil with a concomitant attachment of the flow over most of the upper surface of the airfoil, the rate and amount dependent upon the non-dimensional pitch rate. When the boundary layer can no longer sustain this vorticity accumulation, the dynamic stall vortex is formed near the leading edge aided by the shear layer interaction between the free stream and the boundary layer. Growth and separation of the dynamic stall vortex with its subsequent convection into the wake then occurs. For the single airfoil, this event is followed by a series of dynamic stall induced alternately shed vortices decreasing in strength until a limit cycle indicative of an airfoil at a fixed high angle of attack establishes itself.

For a single airfoil, the process of the formation of the dynamic stall vortex is fundamentally the same across all pitch rates. The major differences are the percentage of chord over which an attached region exists on the suction surface prior to vortex initiation, the angle of attack at which vortex initiation occurs, the strength and cohesiveness exhibited by the dynamic stall vortex, and the time it takes to separate and shed into the wake, all of which increase with non-dimensional pitch rate. At the highest pitch rates, a secondary vortex was observed to form from the separated region near the trailing edge of the upper surface. The cases with the trailing airfoil were no exception; the initiation and development of the dynamic stall vortex over the leading, pitching airfoil are virtually the same for the same non-dimensional pitch rates. In addition, the development of the flowfields about the trailing airfoils due to impingement of the wakes of the pitching airfoils is essentially the same process across pitch rates, varying somewhat in size and strength, but primarily, in time of initiation and development of vortical structures elicited by the unsteady wakes. As with the flow visualization, the pressure measurements, when reduced to pressure coefficients, indicate a strong consistency - particularly at constant values of the non-dimensional pitch rate - among all test conditions. For these reasons, only one set of flow visualization for intermediate pitch rate, $\alpha^+ = 0.2$, is shown.

Flow Visualization

Even though dynamic stall vortex initiation and development are the same for the tandem airfoils as for the single airfoil, dramatic differences begin to occur once the dynamic stall vortex separates from the pitching airfoil. Figures 1 and 2 show visualization of the upper and lower surfaces, respectively, for the case of $\alpha^+ = 0.2$, $\dot{\alpha} = 460^o$/sec, $U_\infty = 20$ fps, Re = 50000. These figures show sequences of two very repeatable events under identical test conditions, one event for the upper surface and one for the lower. They begin at a non-dimensional time of 0.8 (or an angle of attack of 9.2° for the pitching airfoil) beyond pitch initiation. Both figures show flow from left to right with the pitching airfoil on the left and the steaklines from the smoke-wire passing over the top of the trailing airfoil. Flow visualization over the "upper" surface in Figure 1 was accomplished by pitching the upstream airfoil up, or clockwise (CW); conversely, in Figure 2, the upstream airfoil was pitched down, or counter-clockwise (CCW), for visualization of the "lower" surface. For the rest of the discussion on flow visualization, a single letter is used to identify the frames of interest and includes both Figures 1 and 2, unless otherwise specified.

In frame A, the pitching airfoil has reached an angle of attack of 9°, and the series of so-called starting vortices have begun to be shed into the wake, the first of which has impinged on the leading edge of the trailing airfoil. The sense of the starting vortices is CCW for the upper surface in Figure 1 and CW for the lower surface in Figure 2. The disturbances evident at the trailing edge of the upper surface and at the 2/3 chord point of the lower surface are alternately shed vortices from the leading airfoil prior to motion. In frames B,C,D, and E, the only interaction between the shed starting vortices beyond the initial one and the trailing airfoil is on the lower surface, while the flow over the upper surface has become smoothly attached. At an angle of attack of 23° reached by the leading airfoil in frame D, the flow attachment over most of its upper surface effects an entrainment of flow to the region below the lower surface of the trailing airfoil. This causes the pitching airfoil to exhibit characteristics of an unsteady "slat" resulting in attached flow over the lower surface of the trailing airfoil. Frames D through I show a layer of flow of increasing thickness between the lower surface and the vortical wake of the pitching airfoil. This flow has been turned through a large angle causing the trailing airfoil to undergo a negatively increasing aerodynamic angle of attack.

The dynamic stall vortex, formed near the leading edge on the upper surface of the pitching airfoil first appears clearly in frame F, though at this non-dimensional pitch rate it would have been discernible in frame E if the leading edge were visible. It continues to grow in the same manner as for a single airfoil through frame J, and can be seen to contribute greatly to the entrainment of flow around the lower surface of the trailing airfoil. Even though the dynamic stall vortex appears to initiate and develop to this point independently of any intrusion into the flowfield by a trailing airfoil, it is obvious that significant modifications to the wake region have occurred. At this time the most significant events in the interaction between the dynamic stall vortex and the trailing airfoil begin. Above and just upstream of the leading edge of the trailing airfoil, there appears an area where the streaklines split fore and aft. In steady flow, this would appear to be a stagnation point; but for these unsteady flows, it clearly is not since it moves aft. This point will therefore be called a "crux" in the flow. Below, a leading edge vortex similar in nature to a dynamic stall vortex has been initiated. By frame K the dynamic stall vortex has separated from the pitching airfoil and the "crux" has moved to a position above the trailing airfoil almost to the quarter chord; the leading edge vortex continues to grow causing a severe flow curvature in the region between the two airfoils.

At a non-dimensional time of 5.2 in frame L, the leading airfoil has pitched to its maximum angle of attack of 60° and is held there. For a single airfoil, the dynamic stall vortex would now convect in a direction normal to the airfoil chord until it moved out of the separated wake of the airfoil. The flowfield in the vicinity of the trailing airfoil, however, prevents the dynamic stall vortex from doing this. Through frame O and beyond the vortex center convects slowly in a vertical direction until the vortex dissipates. In addition, in frames M-O the dynamic stall vortex loses some of its integrity due to pinching off of portions of it by the upper surface of the trailing airfoil and by the growing leading edge vortex below the leading edge of the lower surface of the trailing airfoil. The leading edge vortex remains stationary and simply grows until it dissipates beyond frame O. At this point, it is clearly the dominant characteristic in the flowfield and may be of greater strength than the dynamic stall vortex since it completely blocks flow between the airfoils. Finally, the "crux" above the upper surface of the trailing airfoil has moved to the trailing edge in frame N.

Pressure Measurements

As in the flow visualization experiments, pressure data were taken first on the upper surface and then on the lower surface. Each set of pressure data, however, represents an ensemble average of 25 events whereas the flow visualization was of a single event. Pressure data were taken for each of the test cases in Table 1, but are compared directly with flow visualization data only for the case of $\alpha^+ = 0.2$, $\dot{\alpha} = 460°/sec$, $U_\infty = 20$ fps, Re = 50000. Pressure coefficients about the trailing airfoil were calculated from the pressure data and are presented as three-dimensional depictions of temporal pressure surfaces where they are plotted versus airfoil chord and non-dimensional time. Figure 3 shows the upper and lower surfaces for the non-dimensional pitch rate case discussed above. As the leading airfoil pitches up, flow over the upper surface remains attached to very high angles of attack. At $\alpha = 23°$ (a non-dimensional time of 2.0), a small (negative) pressure spike is observed near the leading edge of the upper surface of the trailing airfoil with a corresponding (positive) depression at the leading edge of the lower surface. Comparing this with Figures 1 and 2 D, a local curvature in the flow forward of the upper surface of the leading edge exists just prior to entrainment of the flow from the upper to the lower surface. This produces a local acceleration to the flow with a commensurate increase in velocity over the upper leading edge. At this point, as the flow begins to be entrained to the lower surface and the leading airfoil continues its pitch up to 60° (non-dimensional time = 5.2), the upper surface pressure coefficient at and near the leading edge increases, indicating a retardation in the flow. In fact, at a non-dimensional time of 4.4 the "crux" has appeared over the leading edge and accelerates fairly rapidly (to a speed greater than 60% of the freestream velocity) to the trailing edge by a non-dimensional time of 6.0 (see Figure 2 J-N). There occurs a trough of slightly positive values in the upper surface pressure coefficient map that runs diagonally from leading to trailing edge forward in time that seems to be associated with this "crux", but is lagging it slightly. The motion of this "crux" seems evidenced by the sharp rise in upper surface negative pressure coefficient, but is not fully understood.

For the lower surface of the trailing airfoil, once flow has been entrained over it from a non-dimensional time of 2.0 until after

the pitching airfoil has completed its motion, the behavior of the temporal pressure coefficient surface is quite similar to that of the suction surface of a single pitching airfoil. As flow is turned more and more rapidly around the lower leading edge, flow velocity increases producing a high, but relatively broad leading edge negative pressure peak. As the flow transitions to the leading edge vortex at a non-dimensional time of 4.4 (see Figure 2 J), a slight notch appears in the pressure coefficient near the leading edge as it continues on toward its maximum value. As the dynamic stall vortex convects away from the tandem airfoil system and as the trailing airfoil lower surface leading edge vortex dissipates, their influences on the trailing airfoil diminish and the pressure coefficient maps tend toward a quasi-steady state.

Aerodynamic Forces

As mentioned previously, there is a strong consistency across all test conditions in both the flowfield structure about the trailing airfoil and in the magnitudes and shapes of the associated pressure surfaces. Even the magnitudes of the maximum low pressure peaks - shown in Figure 4 - exhibited some consistency across the test matrix. The maximum negative pressure coefficients for the lower surface are roughly double those of upper surface with some slight tendency for increase with α^+. Robinson, et. al.,[14] observed a similar trend at smaller magnitudes for relatively low amplitude harmonically oscillating motions. This is a surprising result considering the wide range of peak pressure coefficients observed on the pitching airfoil from previous studies.[6,19,20,21,22]

Integrating the pressure coefficients provides us with the aerodynamic forces on the trailing airfoil. Figure 5 shows the lift, pressure drag, and quarter-chord moment coefficient for the case of interest (α^+ = 0.2, Re = 50000). The interactions with the vortical wake of the pitching airfoil produce large lifting forces on the trailing airfoil. A small positive peak occurs due to the flow curvature induced by the critical pitching motion. Then, as flow is entrained to the lower surface of the trailing airfoil, negative lift is produced. There is a notch in the lift curve at a non-dimensional time of 4.4, when the leading edge vortex initiates, but the curve continues downward until it reaches a value of -1.40. At this point the leading edge vortex dissipates. For a single pitching airfoil, the dynamic stall vortex sheds into the wake and induces large scale vortex shedding from both the leading and trailing edges before damping out to a pattern of alternate vortex shedding behind a fixed airfoil at high angle of attack. For these cases of tandem airfoils the shedding of the pitching airfoil dynamic stall vortex and the trailing airfoil leading edge vortex apparently elicit similar large scale vortex shedding (though there is no flow visualization to confirm this), evidenced by violent swings in trailing airfoil lift coefficient to values of +0.75 and -0.80 before damping out. These results were generally consistent across the range of values tested with greater similarity among values of constant α^+. At reduced values of the non-dimensional pitch rate smoother curves were produced. The maximum positive and negative values of C_l for all cases are shown in Figure 6. There is a trend toward an increasing $C_{l\ MAX}$ with non-dimensional pitch rate until a value of $\alpha^+ = 0.2$ is reached at which point there is little change. This trend is also consistent with Robinson's[14] results for an oscillating airfoil even though the actual shapes of the lift curves differ markedly.

Pressure drag and quarter-chord moment curves for the trailing airfoil are also plotted in Figure 5. While pressure drag is not substantial - at least compared to the lift coefficients generated - it is, in almost all cases, zero or negative (indicating thrust) over the entire time of data acquisition. The drag curve slopes are small and the peak values across all test cases (see Figure 7) vary little. Moment coefficients are more significant than drag, peak values occurring when there are large lift curve gradients. Maximum positive and negative values are plotted in Figure 8 and follow the same trend as the peak lift values.

Conclusions and Recommendations

Single airfoils pitching at high rates (values of non-dimensional pitch rate from 0.05 to 0.4) from an angle of attack of 0 to 60 degrees produce coherent, repeatable, and energetic dynamic stall vortices over the suction surfaces. These vortices in turn generate large transient aerodynamic forces on the airfoils. The magnitudes of these aerodynamic forces are an increasing function of the non-dimensional pitch rate. While no instrumentation was placed on the pitching airfoil in the presence of a trailing, fixed airfoil, flow visualization studies indicate no significant differences in the local flowfields around the pitching airfoils until the pitching motions were completed. The flowfields downstream of the pitching airfoils were, however, substantially altered by the fixed airfoil.

The interactions between the unsteady vortical wake of the pitching airfoil and the fixed trailing airfoil initially produced a small reverse curvature to the flow which tended to straighten the flow back in the direction of the freestream. Subsequently, the leading airfoil produced an entrainment of the flow below the lower surface of the trailing airfoil which effectively generated significant negative aerodynamic angles of attack. As the dynamic stall vortex formed on the pitching airfoil, the flow was increasingly turned producing increasingly large negative angles of attack - well beyond the static stall angle - on the trailing airfoil. Then, a leading edge vortex forms on the lower surface of the trailing airfoil, similar in many respects to a dynamic stall vortex. The interactions between the dynamic stall vortex, the trailing airfoil, and the leading edge vortex prevent either of the two vortices from convecting downstream. The dynamic stall vortex moves vertically upwards before dissipating, and the leading edge vortex simply grows in place and dissipates.

Pressure distributions around the trailing airfoil were significantly altered by the unsteady wake of the pitching airfoil and the time dependent flowfield induced by it. With the aid of flow visualization, the temporal pressure

signatures could readily be interpreted to determine the sources of the large pressure gradients. Impingement of the dynamic stall vortex on the trailing airfoil and initiation and development of the leading edge vortex could be readily determined. These temporal pressure distributions derived from the development and passage of energetic fluctuating vortical structures produce large oscillating transient loads on the airfoil.

Peak transient forces from half to twice the maximum steady flow values for this airfoil at the Reynolds numbers tested, coupled with the large gradients associated with them, produce serious effects to aerodynamic bodies passing in the immediate wake of airfoils generating unsteady vortex structures. The loads produced are repeatable with surprisingly little variation in magnitudes across all test conditions examined herein. Order of magnitude variations in loading on the pitching airfoil produce only factors of two or three variations in loading on the trailing airfoil with no definitive trend evident. Even so, the magnitudes and time dependencies of the aerodynamic loads produced pose substantial control problems for aerodynamic shapes subjected to them.

Because of the potential for exploiting the high aerodynamic loading generated by forced unsteady vortex flows and because of the potential incorporation of these types of flows into highly maneuverable aircraft with fast moving control surfaces, further investigations in wake interactions are necessary. Near term investigations should examine the effects of pitch amplitude, trailing airfoil spacing, both horizontally and vertically, pitching and trailing airfoil chord variations, trailing airfoil initial angle of attack changes, and trailing airfoil motions.

Acknowledgements

The author appreciates the support of Dr. Michael Robinson of the University of Colorado, Boulder (CU) in fruitful discussions and in producing the figures herein. Dr. Marvin Luttges' permission for the use of the CU 2 ft x 2 ft wind tunnel for the experiments while our own facility was under construction is also greatly appreciated.

References

1. McCrosky, W.J., "Some Current Research in Unsteady Fluid Dynamics - The 1976 Freeman Scholar Lecture," J. Fluids Engr., Vol. 99, Mar 1977, pp. 8-39.

2. McCrosky, W.J., "Unsteady Airfoils," Ann. Rev. of Fluid Mech., 1982, pp. 285-311.

3. Reynolds, W.C., and Carr, L.W., "Review of Unsteady, Driven, Separated Flows," AIAA-85-0527, AIAA Shear Flow Control Conf., 12-14 Mar 1985, Boulder, CO.

4. Ham, N.D., and Garelick, M.S., "Dynamic Stall Considerations in Helicopter Rotors," J. Amer. Heli. Soc., Vol. 13, No. 2, Apr 1968, pp. 49-55.

5. Robinson, M.C., and Luttges, M.W., "Unsteady Separated Flow: Forced and Common Vorticity About Oscillating Airfoils," Proceedings: Workshop on Unsteady Separated Flows, 10-11 Aug 1983, U.S. Air Force Academy, CO, pp. 117-126.

6. Francis, M.S., Keesee, J.E., and Retelle, J.P., "An Investigation of Airfoil Dynamic Stall with Large Amplitude Motions," FJSRL-TR-83-0010, Oct 1983.

7. Walker, J.M., Helin, H.E., and Strickland, J.H., "An Experimental Investigation of an Airfoil Undergoing Large Amplitude Pitching Motions," AIAA J., Vol. 23, No. 8, Aug 1985, pp. 1141-1142, also AIAA-85-0039, AIAA 23rd Aerospace Sciences Mtg., 14-17 Jan 1985, Reno, NV.

8. Padakannaya, R., "Experimental Study of Rotor Unsteady Airloads Due to Blade-Vortex Interactions," NASA CR-1909, Nov 1971.

9. McAlister, K.W., and Tung, C., "Airfoil Interaction With an Impinging Vortex," NASA TP-2273, AVSCOM TR-83-A-17, 1984.

10. Favier, D., Maresca, C., and Rebont, "Dynamic Stall of NACA 0012 Airfoil Due to Fluctuations of Velocity and Incidence," AIAA-81-1288, AIAA 14th Fluid and Plasma Dynamics Conf., 23-25 Jun 1981, Palo Alto, CA.

11. Telionis, D.P., and Poling, D.Z., "The Response of Airfoils to Periodic Disturbances---The Unsteady Kutta Condition," AIAA J., Vol. 24, No. 2, Feb 1986, pp. 193-199, also AIAA-84-0050, AIAA 22nd Aerospace Sciences Mtg., 9-12 Jan 1984, Reno, NV.

12. Srinivasan, G.R., McCroskey, W.J., and Baeder, J.D., "Aerodynamics of Two-Dimensional Blade-Vortex Interaction," AIAA J., Vol. 24, No. 10, Oct 1986, pp. 1569-1576, also AIAA-85-1560, AIAA Fluid Dynamics, Plasma Dynamics and Lasers Conf., 16-18 Jul 1985.

13. Booth, E.R., "Surface Pressure Measurement During Low Speed Two-Dimensional Blade-Vortex Interaction," AIAA-86-1856, AIAA 10th Aeroacoustics Conf., 9-11 Jul 1986, Seattle, WA.

14. Robinson, M.C., Helin, H.E., and Luttges, M.W., "Control of Wake Structure Behind an Oscillating Airfoil," AIAA-86-2282, AIAA Fluid Mechanics, Plasma Dynamics, and Lasers Conference, May 1986, Atlanta, GA.

15. Rockwell, D., "Unsteady Loading of Leading-Edges in Unstable Flows: An Overview," AIAA-84-2306, AIAA/NASA 9th Aeroacoustics Conf., 15-17 Oct 1984, Williamsburg, VA.

16. Huang, M.-K., and Chow, C.-Y., "Trapping of a Free Vortex by Joukowski Airfoils," AIAA J., Vol. 20, No. 3, Mar 1982, pp. 292-298.

17. Chow, C.-Y., Huang, M.-K., and Yan, C.-Z., "Unsteady Flow About a Joukowski Airfoil in the Presence of Moving Vortices," AIAA J., Vol. 23, No. 5, May 1985, pp. 657-658, also AIAA 83-0129, AIAA 21st Aerospace Sciences Mtg., 10-13 Jan 1983, Reno, NV.

. Wu, J.C., Sankar, N.L., and Hsu, T.M., nsteady Aerodynamics of an Airfoil Encountering Passing Vortex," AIAA-85-0203, AIAA 23rd rospace Sciences Mtg., 14-17 Jan 1985, Reno, NV.

. Walker, J.M., Helin, H.E., and Chou, D.C., nsteady Surface Pressure Measurements on a tching Airfoil," AIAA-85-0532, AIAA Shear Flow ntrol Conf., 12-14 Mar 1985, Boulder, CO.

. Walker, J.M., "Forced Unsteady Vortex Flows :ven by Pitching Airfoils," PJSRL-TR-86-0010, 1986.

21. Francis, M.S., and Keesee, J.E., "Airfoil Dynamic Stall Performance with Large-Amplitude Motions," AIAA J., Vol. 23, No. 11, Nov 1985, pp. 1653-1659.

22. Jumper, E.J., Schreck, S.J., and Dimmick, R.L., "Lift-Curve Characteristics for an Airfoil Pitching at Constant Rate," AIAA-86-0117, AIAA 24th Aerospace Sciences Mtg., 6-9 Jan 1986, Reno, NV.

23. Cook, R.J., "Similarity Conditions for Flows About Pitching Airfoils," to be submitted to AIAA J. as TN, Jan 1987.

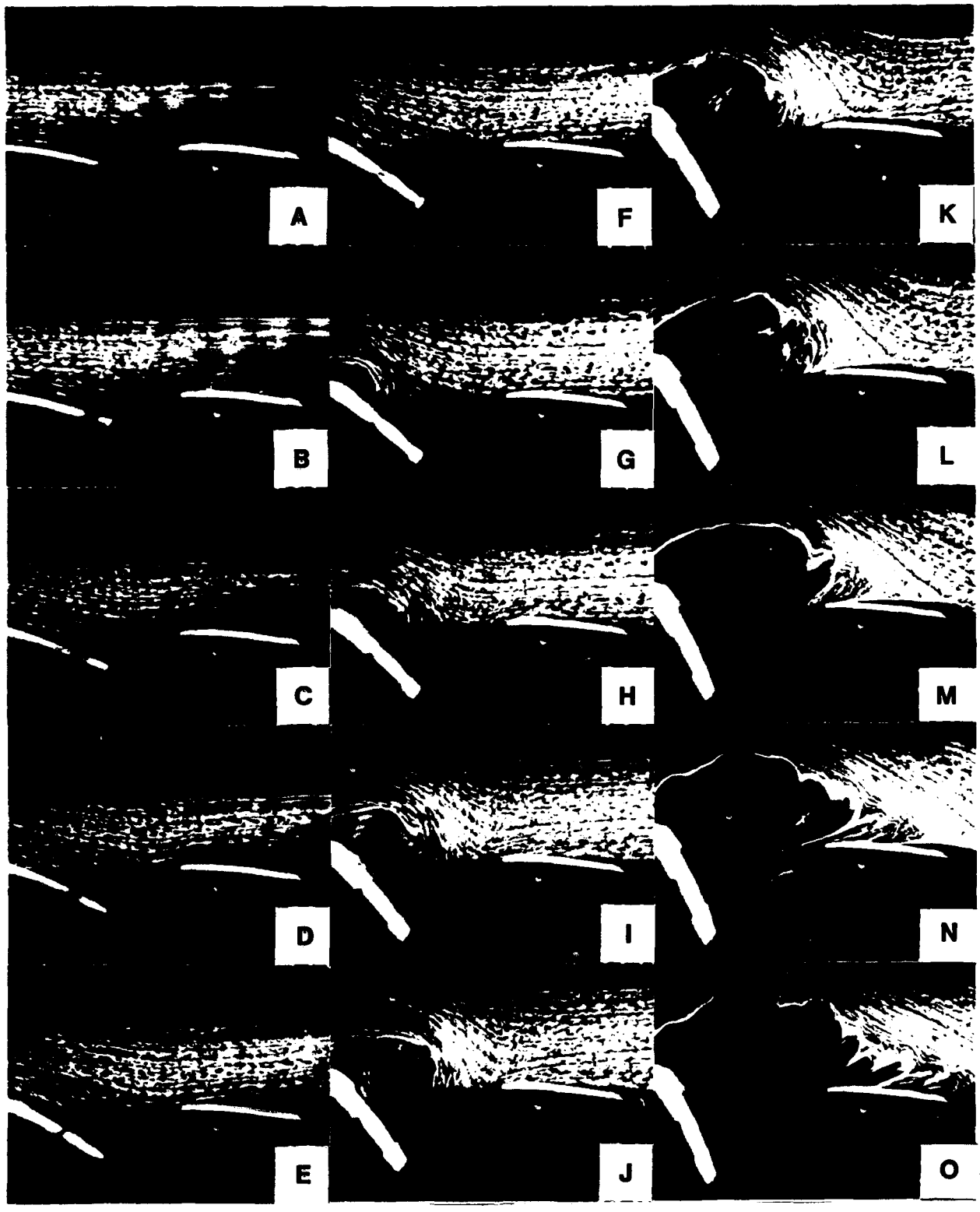

Figure 1. Flow Visualization, Upper Surface, Re = 50000
Upstream airfoil, $\alpha^+ = 0.2$
Downstream airfoil, $\alpha = 0$

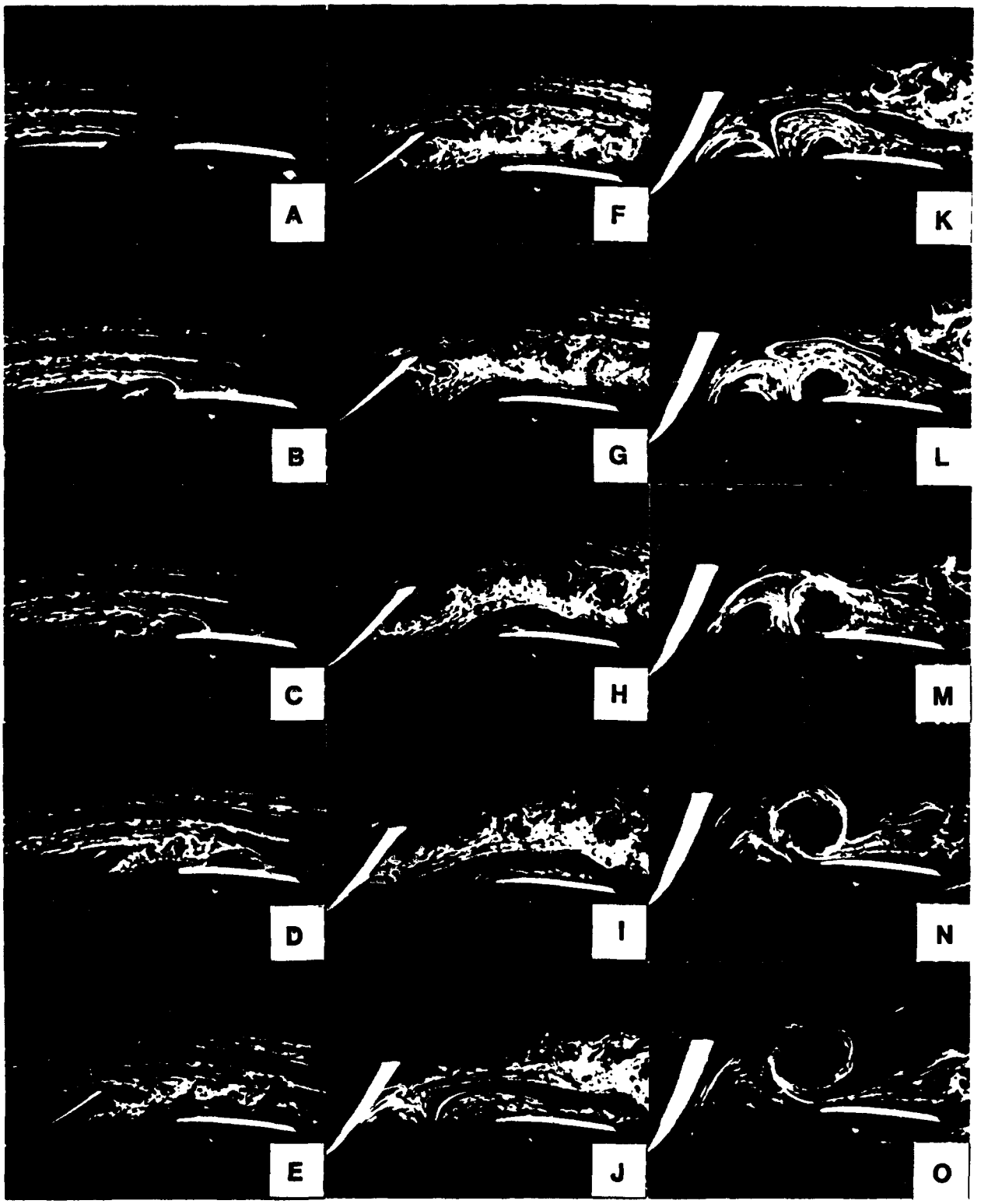

Figure 2. Flow Visualization, Lower Surface, Re = 50000
Upstream airfoil, $\alpha^+ = 0.2$
Downstream airfoil, $\alpha = 0$

Alpha+ = 0.2, Re = 50000, Upper Surface

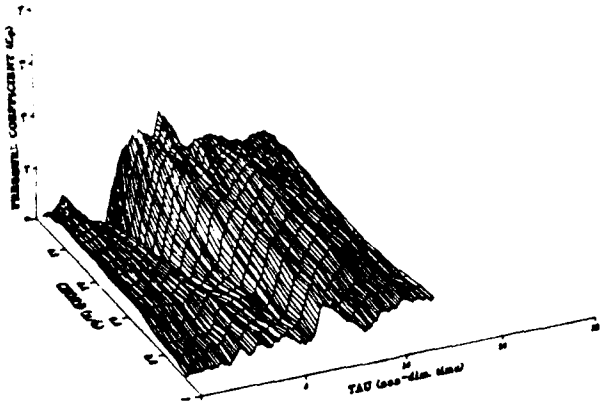

Alpha+ = 0.2, Re = 50000, Lower Surface

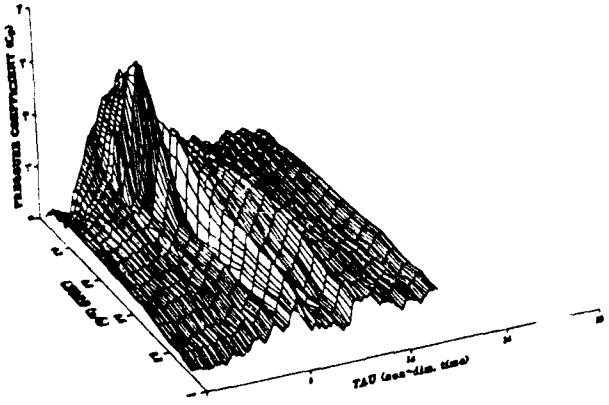

Figure 3. Downstream Airfoil Unsteady Pressure Coefficient Distributions
Re = 50000, α = 0 (upstream airfoil α^+ = 0.2)

Peak Pressure Coefficients

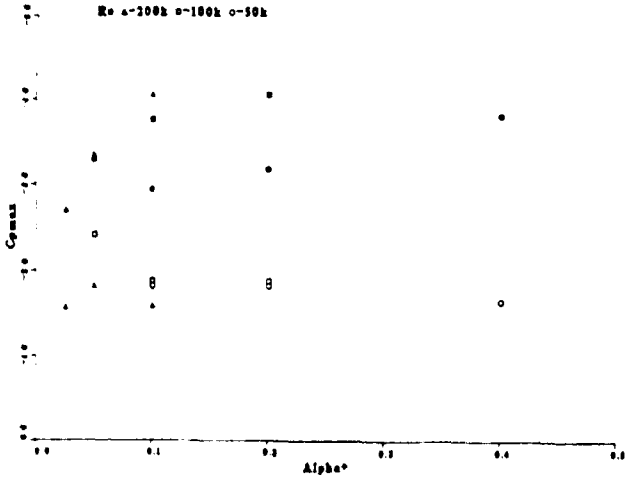

Figure 4. Maximum Pressure Peaks Induced by Airfoil/Wake Interactions

ALPHA+ = 0.2, RE = 50000

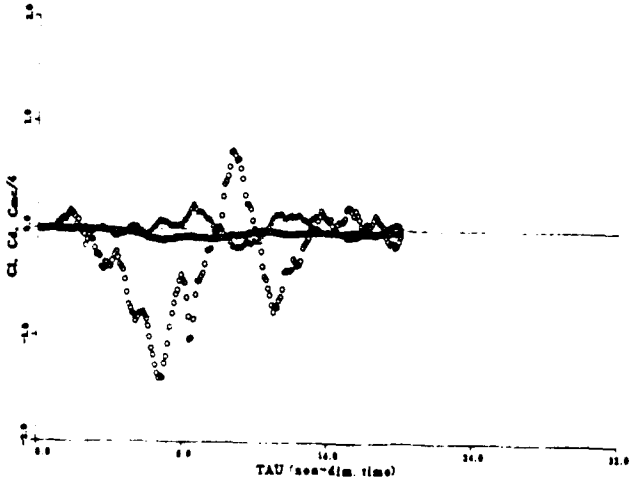

Figure 5. Downstream Airfoil Lift, Pressure Drag, and Quarter-chord Moment Coefficients
Re = 50000, α = 0 (upstream airfoil α^+ = 0.2)

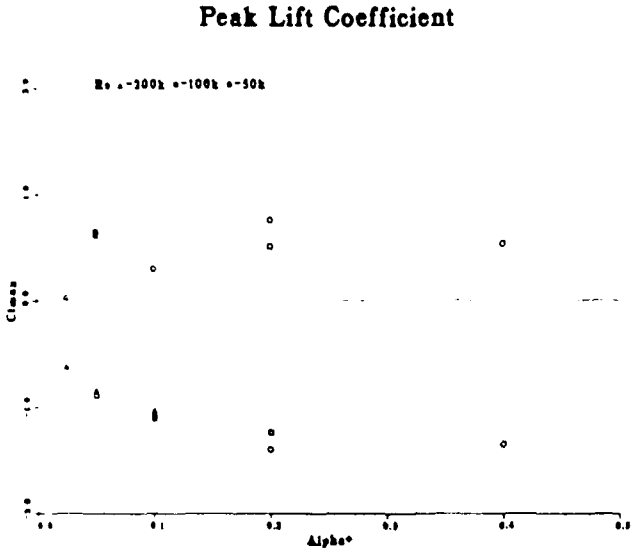

Figure 6. Maximum Lift Coefficient Transients Induced by Airfoil/Wake Interactions

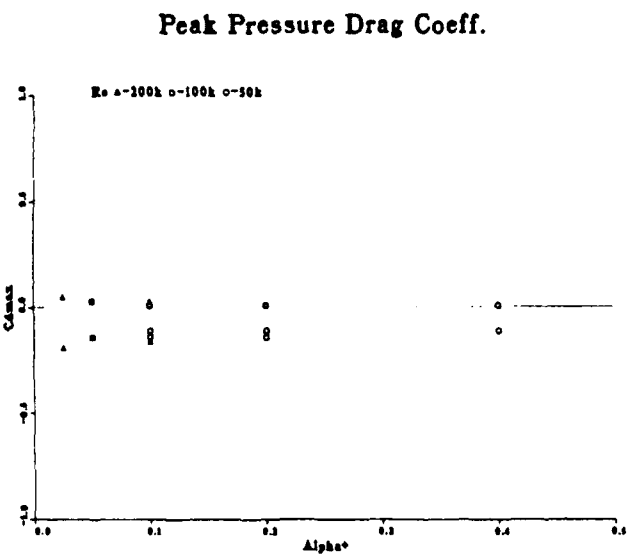

Figure 7. Maximum Pressure Drag Coefficient Transients Induced by Airfoil/Wake Interactions

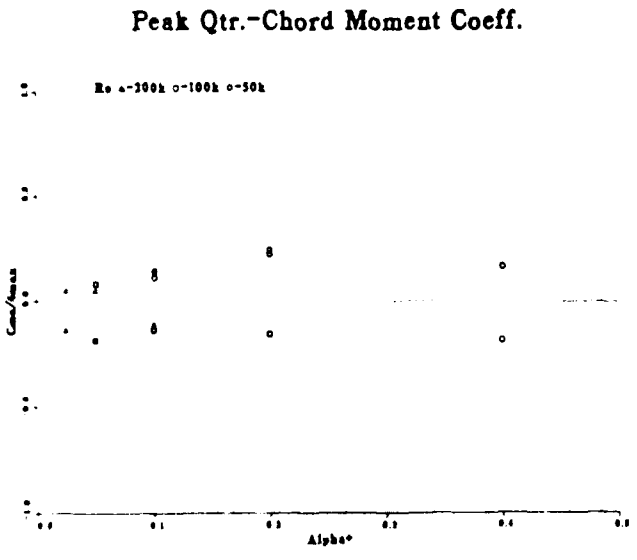

Figure 8. Maximum Quarter-chord Moment Coefficient Transients Induced by Airfoil/Wake Interactions